ROYAL SOCIETY OF CHEMISTRY

PAPER

A hillock-like phenomenon with low friction and adhesion on a graphene surface induced by relative sliding at the interface of graphene and the SiO$_2$ substrate using an AFM tip

Na Fan, [iD] †[a] Jian Guo,†[ab] Guangyin Jing, [iD] [c] Cheng Liu,[a] Qun Wang,[a] Guiyong Wu,[a] Hai Jiang[a] and Bei Peng*[a]

Graphene demonstrates high potential as an atomically thin solid lubricant for sliding interfaces in industry. However, graphene as a coating material does not always exhibit strong adhesion to any substrates. When the adhesion of graphene to its substrate weakens, it remains unknown whether relative sliding at the interface exists and how the tribological properties of the graphene coating changes. In this work, we first designed a method to weaken the adhesion between graphene and its SiO$_2$ substrate. Then the graphene with weakened adhesion to its substrate was rubbed using an AFM tip, where we found a novel phenomenon: the monolayer graphene not only no longer protected the SiO$_2$ substrate from deformation and damage, but also prompted the formation of hillock-like structures with heights of approximately tens of nanometers. Moreover, the surface of the hillock-like structure exhibited very low adhesion and a continuously decreasing friction force *versus* sliding time. Comparing the hillock-like structure on the bare SiO$_2$ surface and the proposed force model, we demonstrated that the emergence of the hillock-like structure (with very low adhesion and continuously decreasing friction) was ascribed to the relative sliding at the graphene/substrate interface caused by the mechanical shear of the AFM tip. Our findings reveal a potential failure of the graphene coating when the adhesion strength between graphene and its substrate is damaged or weakened and provide a possibility for *in situ* fabrication of a low friction and adhesion micro/nanostructure on a SiO$_2$/graphene surface.

Introduction

Recently, two-dimensional (2D) materials have attracted significant interest due to their ability to reduce friction further due to the weak interlayer van der Waals interaction.[1–3] Accordingly, atomically thin graphene indicates promising prospects for the lubrication of micro/nano-electromechanical systems (MEMS/NEMS) because of its excellent tribological properties;[4–8] hence, the nanotribological study of graphene has gradually become a popular research topic relating to 2D materials. Many experimental studies have revealed the unique nanotribological properties of graphene, namely, the friction force of graphene decreasing with the increasing numbers of layers.[4,9] Some researchers have also reported results regarding superlubricity and ultralow friction of graphene,[10–14] such as

superlubric sliding of graphene nanoscrolls on diamond like carbon[11] and superlubric sliding of graphene-coated microspheres on graphene.[12]

The adhesion between graphene and its substrate has been found to play an important role in the nanotribological behaviour of graphene.[15,16] Zeng *et al.*[15,16] indicated that the friction force on the graphene surface could be controlled by changing the adhesion strength between graphene and its substrate by plasma treatment of the substrate. In addition, it was found that different substrates (such as Ni, SiO$_2$, and PDMS) have different influences on the friction force of graphene, due to significantly different adhesion energies at the graphene/substrate interfaces.[17,18] Conversely, the direct measurement method of adhesion properties between graphene and different substrates involving silicon and metal substrates was successively proposed.[19–21] In most cases, graphene cannot be directly grown on the desired substrates but first needs to be grown on another substrate and then physically transferred onto the target substrate.[22,23] Because the adhesion strength between graphene and the target substrate depends highly on the transfer process, the nanotribological properties of graphene may be compromised by this physical transfer process. However, tribological

[a]*School of Mechanical and Electrical Engineering, University of Electronic Science and Technology of China, Chengdu 611731, China. E-mail: beipeng@uestc.edu.cn*

[b]*School of Mechanical Engineering, University of South China, Hengyang 421001, China*

[c]*National Key Laboratory and Incubation Base of Photoelectric Technology and Functional Materials, School of Physics, Northwest University, Xi'an 710069, China*

† Equal contributions from the authors.

studies have been conducted recently in which graphene adheres well to its substrate. Given that graphene does not always have strong adhesion to many substrates, the tribological properties of graphene in the case of weakened adhesion are unclear.

It has been reported that the adhesion of graphene to the SiO_2 substrate is weaker than that to metal substrates;[17] therefore, it is easier to weaken the adhesion between graphene and the SiO_2 substrate. In this study, we first designed an experiment to reduce the adhesion strength at the interface of graphene and its SiO_2 substrate. Then, we found that graphene would not protect its SiO_2 substrate well due to producing the so-called friction-induced hillock,[24,25] but prompt the formation of a higher hillock-like structure on the SiO_2/graphene surface. Moreover, we conducted comparative analysis between the friction and adhesion forces for four different surfaces, as follows: a bare SiO_2 substrate, graphene covered on the SiO_2 substrate, graphene suspended on the grooves, and a SiO_2/graphene hillock-like structure. The results indicated that the surface of the hillock-like structure exhibited very low adhesion and continuously decreasing friction versus sliding time. Comparing the hillock-like structure on bare SiO_2 and the proposed force model, we demonstrated that the emergence of the hillock-like structure (with very low adhesion and continuously decreasing friction) was related to the relative sliding at the interface of graphene and the SiO_2 substrate.

Previous studies have found that the environmental sensitivity,[26,27] edge effect,[28] and defects[29,30] of graphene can cause the failure of the graphene coating. Our work revealed another potential failure of graphene: when the adhesion strength between graphene and its substrate is weakened (or even broken), a relative sliding at the interface of graphene/substrate occurs, along with the formation of a hillock-like structure on the SiO_2/graphene surface. Conversely, our work could offer the possibility of in situ fabrication of the micro/nanostructure with low friction and adhesion on the SiO_2/graphene surface, which may have potential applications in micro- and nano-devices, such as miniature gear and micro turbines or any other friction pairs on the micro- and nano-scale.

Results and discussion

(I) Hillock-like phenomena on the SiO_2/graphene surface

To study the nanotribological properties of graphene when the adhesion strength between graphene and the SiO_2 substrate was weakened, we designed and performed a corresponding experiment, as shown in Fig. 1. Fig. 1a shows that the monolayer graphene was successfully transferred on the SiO_2 substrate patterned with a groove-array structure. It can be noted that parts of the graphene were suspended on the grooves (namely suspended graphene) and the other parts adhered well to the SiO_2 substrate surface (namely supported graphene). AFM experiments were conducted on both the suspended graphene region and supported graphene region. Fig. 1b–d show in detail the generation procedure of the hillock-like structure: (i) first, the suspended graphene was rubbed using an AFM Si tip under a certain normal load (Fig. 1b). As a result, the adhesion strength between the graphene and SiO_2 substrate is gradually weakened by the mechanical shear of the AFM tip. (ii) Second, the suspended graphene slides along the SiO_2 substrate, resulting in more graphene sinking into the groove where the tip rubs, where the adhesion strength between the graphene
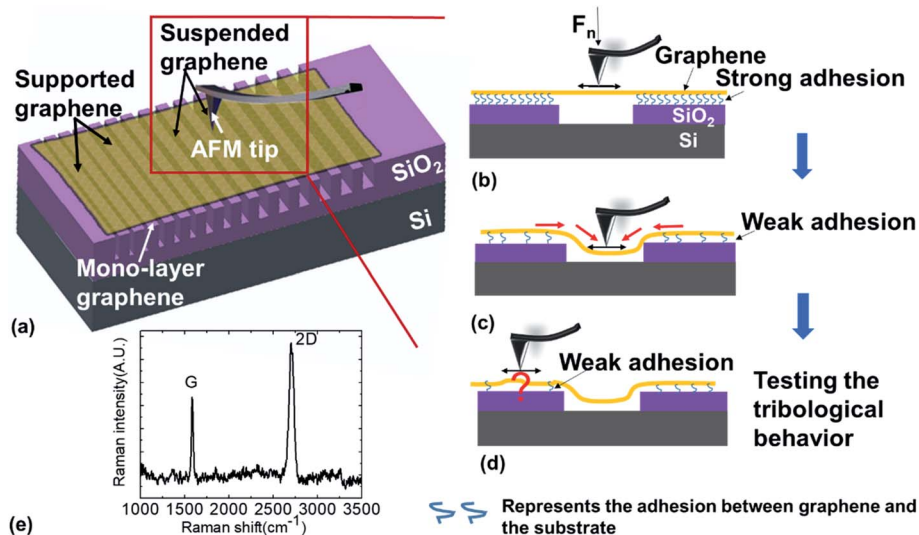

Fig. 1 Schematic diagram showing the experimental process. (a) Schematic structure of the monolayer graphene transferred onto the groove-patterned SiO_2 substrate surface, where some of the graphene is suspended in the grooves and some adheres to the pattern-less SiO_2 substrate surface. (b–d) Schematic drawing of the experimental design with the interactions the between silicon tip and suspended monolayer graphene. First, a friction experiment is performed on the suspended graphene surface using an AFM Si tip; as a result, the adhesion strength would be gradually weakened by mechanical shear action. Second, the suspended graphene slides along the groove and sinks (to some extent) into the groove. Finally, the silicon tip rubbed the supported graphene region and tested the tribological behaviour of the new SiO_2/graphene surface. (e) Typical Raman spectra with the intensity ratios of 2D and G peaks demonstrating that the sample is monolayer graphene films.

and SiO$_2$ substrate changes from strong to weak (Fig. 1c). (iii) Finally, the AFM tip rubs the supported graphene region (Fig. 1d), testing the tribological behaviour of the new SiO$_2$/graphene surface with weak adhesion at the interface of the supported graphene and SiO$_2$ substrate. Raman spectral analysis results indicated that the graphene sample was monolayer graphene, determined from the intensity ratios of 2D and G peaks, as shown in Fig. 1e.
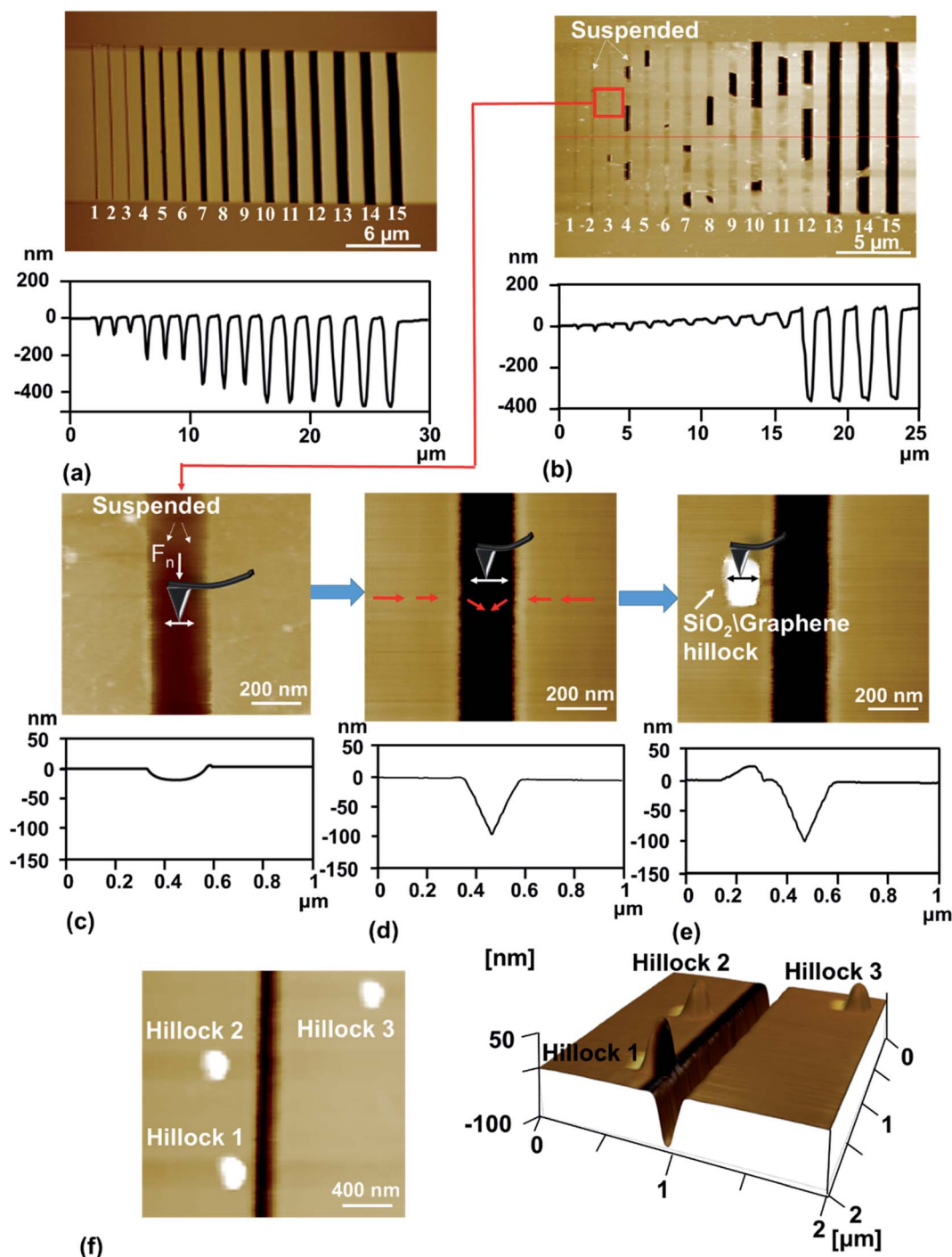

Fig. 2 Formation process of the hillock-like structure on the supported graphene surface. (a) AFM image (top) and cross-sectional profile (bottom) of the groove-patterned SiO$_2$ substrate. (b) AFM image (top) and cross-sectional profile along the red line (bottom) of monolayer graphene transferred onto the groove-patterned SiO$_2$ substrate. (c) AFM image and the cross-sectional profile showing the *in situ* region before silicon tip rubbing of the suspended graphene. (d) AFM image and cross-sectional profile showing the *in situ* region after silicon tip rubbing of the suspended monolayer graphene. (e) AFM image and the cross-sectional profile showing the *in situ* region after tip rubbing of the supported graphene surface near the groove, where a hillock-like structure with a height of ∼20 nm is observed. (f) 2D topography (left) and 3D topography (right) of three hillock-like structures produced on the sliding surface of the suspended monolayer graphene.

Formation and evolution of the hillock-like structure on the SiO₂/graphene surface. Usually, when performing friction experiments on a graphene surface with good adhesion to the SiO₂ substrate, graphene as a coating can protect the SiO₂ substrate from the mechanical shear well; hence, the hillock-like structure cannot occur. For a sharp comparison, when the adhesion strength between graphene and the SiO₂ substrate was weakened, there was a possibility of forming the hillock-like structure *in situ* by rubbing using the AFM tip, as can be seen in Fig. 2. Fig. 2a shows the AFM image (top) and cross-sectional profile (bottom) of the 15 groove structures numbered 1–15 on the SiO₂ substrate, which can be divided into five groups according to width and depth (grooves 1–3, 300 nm width by 100 nm depth; grooves 4–6, 600 nm width by 200 nm depth; grooves 7–9, 800 nm width by 400 nm depth; grooves 10–12, 1200 nm width by 450 nm depth; and grooves 12–15, 1400 nm width by 470 nm depth). Fig. 2b shows the AFM image (top) and cross-sectional profile along the red line (bottom) of monolayer graphene transferred onto the groove-patterned SiO₂ substrate. It can be clearly observed that most of the groove region was covered by the monolayer graphene, suggesting that the monolayer graphene was well suspended above these grooves with widths lower than ∼800 nm. Fig. 2c shows that the suspended graphene was rubbed using an AFM tip under a normal load F_n of 3 μN and sliding cycles ($N = 10$) on a 100×100 nm area where scanning one AFM map is one sliding cycle. After AFM tip rubbing (as shown in Fig. 2d) the suspended graphene that was originally laid flat on the groove collapsed and sank into the groove to a depth of ∼80 nm, indicating that the monolayer graphene that adhered to the SiO₂ substrate well originally was pulled and dragged by the AFM tip. Here, after AFM tip rubbing, the supported graphene region under a normal load F_n of 150 nN and sliding cycles ($N = 10$) over an area of 100×100 nm formed a hillock-like structure with a height of ∼20 nm and bottom area of 80×150 nm on the sliding *in situ* monolayer graphene, as shown in Fig. 2e. To investigate whether the generation of such a hillock-like structure could be repeated experimentally, we repeated the experiment five times (some of the repeated hillock-like structures emerged as seen in Fig. 2f). It can be observed (Fig. 2f) that another three hillock-like structures with sizes (height × length × width) of $50 \times 80 \times 150$ nm, $35 \times 80 \times 120$ nm, and $25 \times 80 \times 100$ nm, respectively, were produced on the sliding surface under the conditions of a normal load F_n of 150 nN, sliding cycles ($N = 10$) and a sliding area of 100×100 nm.

To investigate the stability and evolution of the hillock-like structure on the SiO₂/graphene surface further, we conducted scratching and indentation experiments with the AFM Si tips. First, scratching experiments were carried out on the surface of the hillock structure under a normal load F_n of 150 nN and sliding cycles ($N = 10$) over a sliding area of 50×50 nm. As illustrated in Fig. 3, the height of the hillock-like structure increased from ∼20 nm (Fig. 3a) to ∼60 nm (Fig. 3b) after scratching. After continuing to scratch the hillock-like structure in the same way, the height of the hillock-like structure decreased from ∼60 nm (Fig. 3b) to ∼45 nm (Fig. 3c). Subsequently, an indentation experiment was performed on the hillock-like structure surface under a normal load F_n of 1 μN and different numbers of indentation cycles of 10, 50 and 100, as shown in Fig. 4. Fig. 4a presents a hillock-like structure with a height of ∼20 nm, produced under a normal load F_n of 150 nN and sliding cycles ($N = 10$). It was observed that after 50 indentations, a 1 nm deep pit was generated on the surface of the hillock-like structure (Fig. 4c). A deeper pit formed when the number of the indentation cycles was increased to 100 (Fig. 4d). By contrast, when the same indentation and scratching tests were performed on the original SiO₂/graphene surface with good adhesion, the pit and the hillock-like structure could not form in the indentation and scratching region, which suggests that the mechanical properties of the hillock-like structure were notably different from those of the original SiO₂/graphene. Because the hardness of graphene is much higher than that of
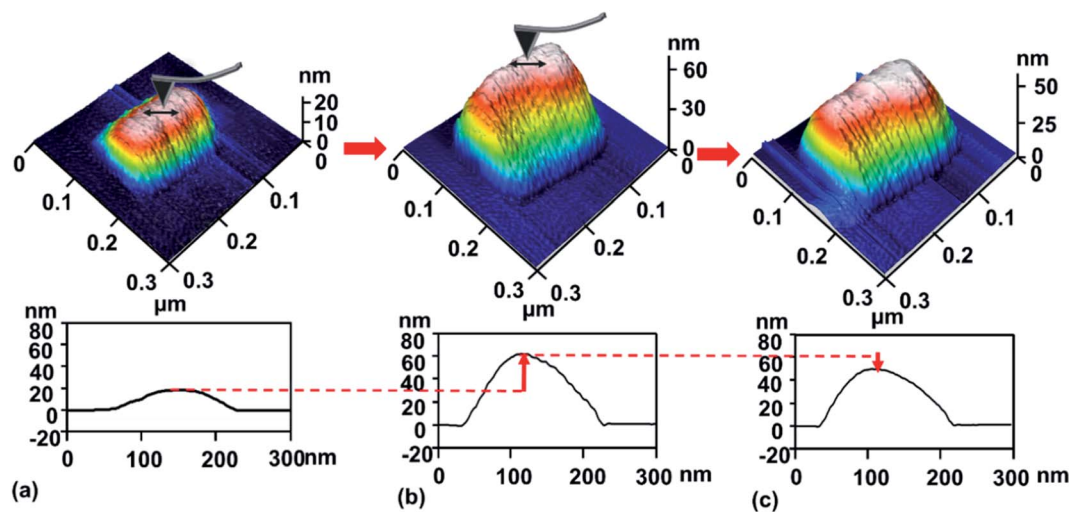
Fig. 3 Scratching tests on the hillock-like structure surface. (a) A hillock-like structure with a height of ∼20 nm on the supported graphene surface; (b) and (c), respectively, show that after the scratching test, the height of the hillock-like structure increased from ∼20 nm to ∼60 nm, and then decreased from ∼60 nm to ∼45 nm.
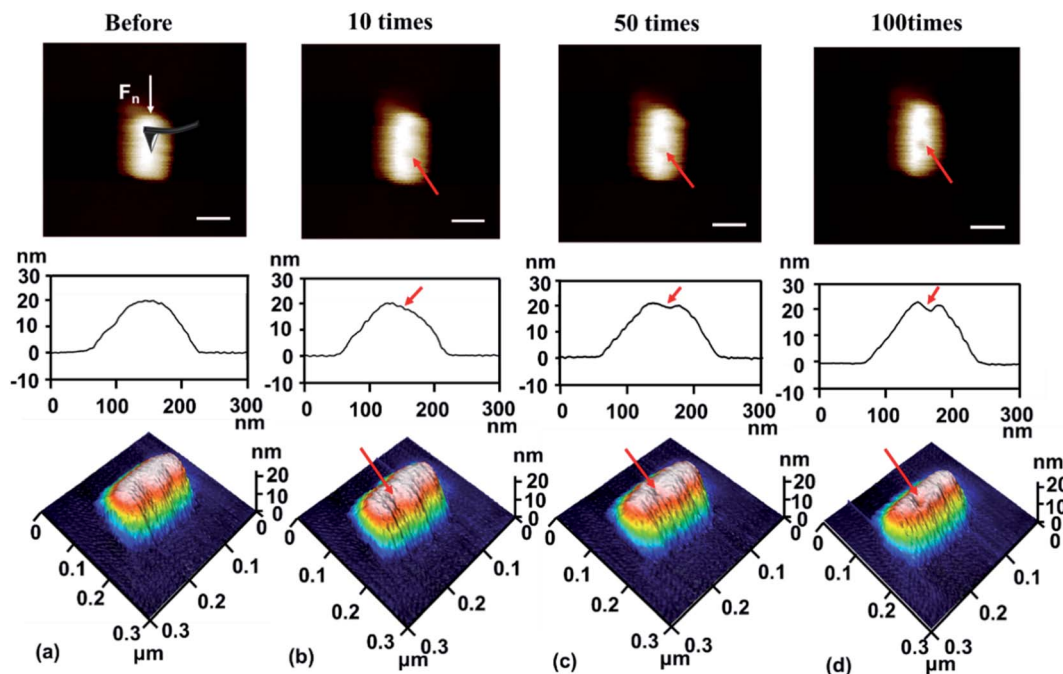
Fig. 4 Indentation tests with different numbers of indenting cycles on the hillock-like structure surface. (a) A hillock-like structure on the supported monolayer graphene surface before the indentation tests; (b), (c), and (d) show the topography variation of the hillock-like structure with the number of indentation cycles of 10, 50, and 100 times, respectively. The applied normal load F_n during such tests was 1 μN. The scale bars in the AFM images were 50 nm.

the AFM Si tip, we considered that the hillock-like structure was related to the thick SiO_2 substrate rather than the deformation of graphene.

Formation of the hillock-like structure on the bare SiO_2 surface. To investigate the formation mechanisms of hillock-like phenomena on SiO_2/graphene further, we performed the

AFM tip rubbing experiment on the bare SiO_2 substrate surface (without the graphene coating) and found a hillock-like structure with a much lower height compared to the hillock-like structure on the SiO_2/graphene surface. Fig. 5 shows the effect of a normal load on the friction-induced hillock structure on the SiO_2 surface. When the normal load was 250 nN, a slight
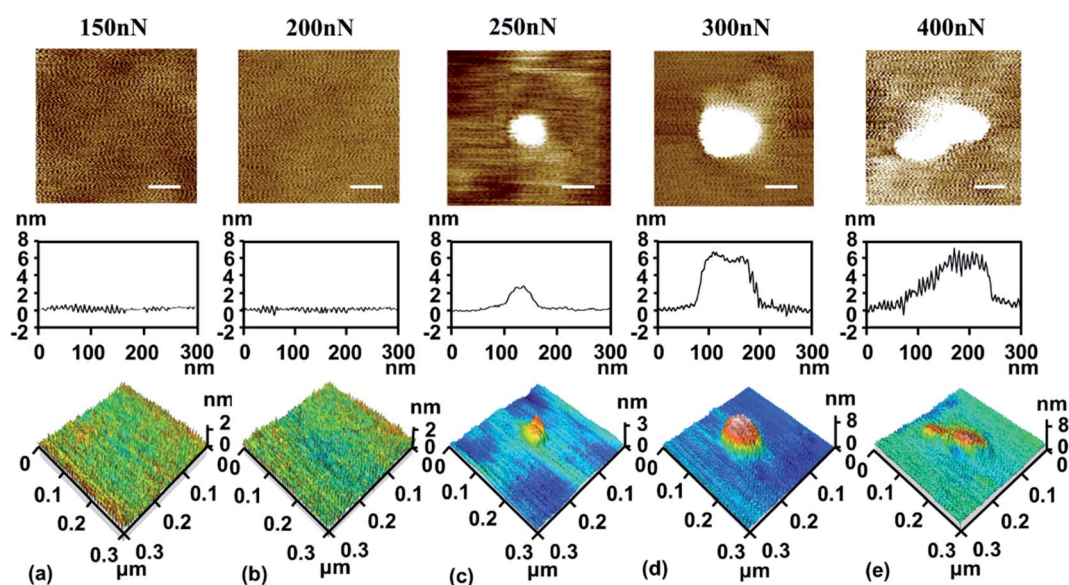

Fig. 5 Effect of normal load on the friction-induced hillock structure on the bare SiO_2 surface. The sliding tests are performed on five regions with an area of 100 nm × 100 nm under the normal loads of 150 nN, 200 nN, 250 nN, 300 nN and 400 nN, respectively. The scale bars in this figure are 60 nm.

hillock-like structure with a height of ~3 nm was observed on the SiO_2 surface, while no hillock structure formed when the normal load was lower than 250 nN. When the normal load was increased from 250 to 400 nN, the height of the hillock-like structure increased from 3 to 8 nm. However, the height of the structure did not increase when we continued to increase the normal load, indicating that the maximum height of such a structure on bare SiO_2 was less than 10 nm, far below that of the hillock-like structure on the SiO_2/graphene surface.

By comparing Fig. 2 and 5, the difference between the hillock-like structure on the SiO_2/graphene surface and the hillock structure on the bare SiO_2 surface can be clearly seen. We speculated that after AFM tip rubbing, the suspended graphene under a given normal load and number of sliding cycles, would demonstrate a weakened adhesion strength between graphene and its SiO_2 substrate, and relative movement would occur at this interface. Thus, when the AFM tip rubbed the supported graphene, the SiO_2 substrate was not only rubbed by

the tip but the tip and the attached graphene worked together. In other words, the tip and the attached graphene—with some warping—constituted a new 'tip' to rub the SiO_2 substrate; because of the stronger mechanical interaction induced by this 'tip' in comparison to the Si tip only, the hillock-like structure would be more easily produced.

Here, we summarised the different states of the bare SiO_2 surface, strong-adhesion SiO_2/graphene surface, and weak-adhesion SiO_2/graphene surface when rubbed using the Si tip, as shown in Fig. 6. Fig. 6a shows that a friction-induced hillock structure could be directly produced on the SiO_2 surface after Si tip rubbing, suggesting that some deformation or lattice change has taken place in SiO_2 crystals, which was also discovered in previous studies.[24,25] In the case of strong adhesion between graphene and its SiO_2 substrate, graphene as a coating can protect the SiO_2 substrate well against the mechanical shear of the Si tip, thus preventing the formation of the hillock-like structure, as shown in Fig. 6b. In fact, it is difficult to
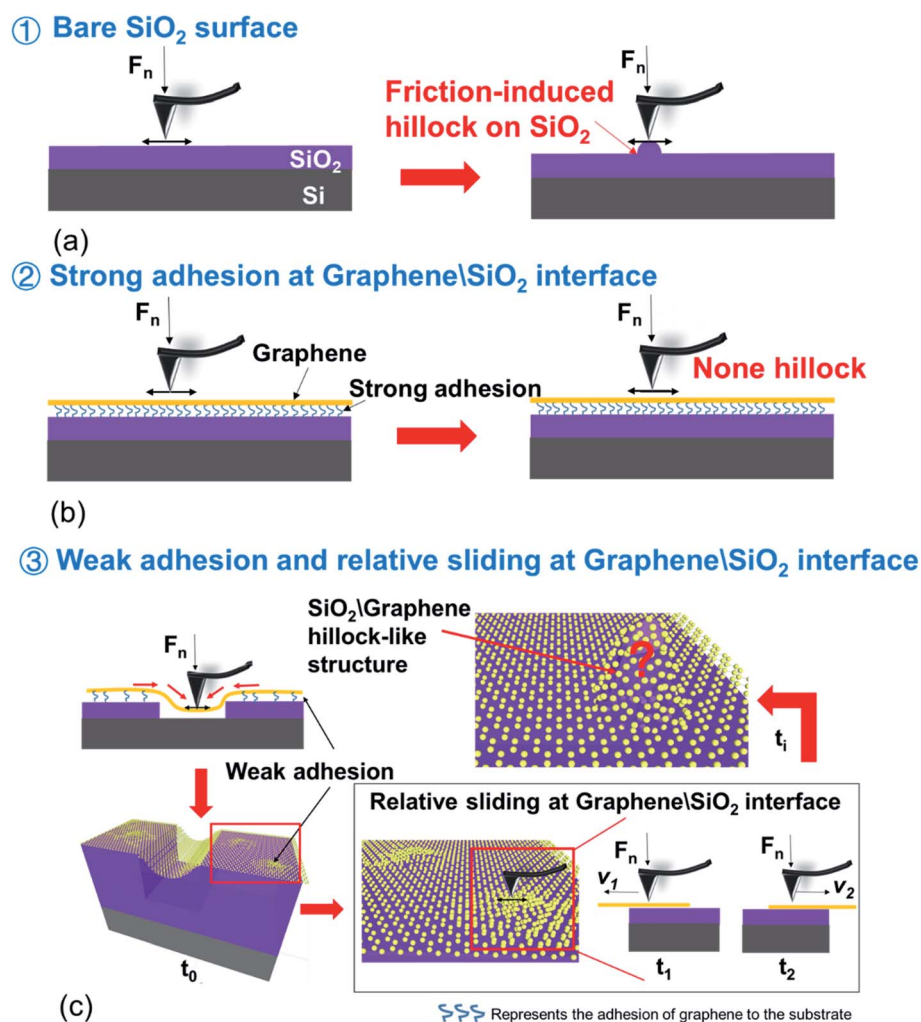

Fig. 6 Three different situations of the friction behaviour when rubbed using the AFM tip. (a) Bare SiO_2 surface rubbed with the AFM tip and a corresponding friction-induced hillock appearing on the SiO_2 surface. (b) No hillock-like structure occurs when a graphene coating covers the SiO_2 surface where the graphene adheres well on its substrate. (c) A relative sliding at the interface of the graphene and SiO_2 substrate would occur when the adhesion at the interface is weakened, which results in a SiO_2/graphene hillock-like structure.

guarantee that the graphene always adheres well with its substrate in such an application scenario. To understand what would happen if the tip rubbed the graphene adhered weakly with its substrate, we designed an experiment as shown in Fig. 6c. First, we rubbed the suspended graphene with an AFM tip and made the suspended graphene sink into the groove. As a result, the adhesion strength between graphene and the SiO_2 substrate was weakened, causing the graphene supported on the substrate to move with the substrate. The initial time when the adhesion of graphene to the substrate became weak is denoted as time t_0. As the tip rubs against the graphene surface, the graphene slides relative to the SiO_2 substrate, denoted as time t_1. With the continuous rubbing of the AFM tip, the adhesion of graphene to the substrate becomes weaker and weaker, denoted as time t_2, at which graphene directly interacts with the substrate during the movement of the tip. Finally, a hillock-like structure with a height of approximately tens of nanometers forms *in situ* on the sliding monolayer graphene. The SiO_2/graphene hillock-like structure may be formed from the deformed SiO_2 or combined with the puckering graphene as mentioned in the previous study[31–33] and the deformed SiO_2.

Compared with these three different situations described, a hypothesis has been proposed that when the adhesion of graphene to its substrate weakened, it could result in the relative sliding occurring at the interface of graphene and the substrate. In order to prove the hypothesis and demonstrate the SiO_2/graphene hillock-like structure, we conducted friction force and adhesion force tests as follows.

(II) A relative sliding at the interface of the graphene and SiO_2 substrate

In order to prove the hypothesis that the relative sliding would occur at the interface of graphene and the substrate when the adhesion of graphene to its substrate is weakened, we measured the friction force (Fig. 7) on four different surfaces, namely the SiO_2 surface, supported graphene surface, suspended graphene surface, and hillock-like structure surface. Fig. 7a and b show the variation of friction force as a function of the sliding time on the four different surfaces, where the friction force value was obtained in the area-scan mode with an area of 100 × 100 nm using AFM, under the normal loads of 5 and 10 nN. It was found that the average friction force values on the four different surfaces had the following relationship: the SiO_2 substrate > the supported graphene > the suspended graphene > the hillock-like structure. In addition, it is notable that the friction force on the hillock-like structure surface demonstrated a significantly different situation compared to that on the other three surfaces: the friction force gradually decreased with the sliding time, while the friction forces on the other three surfaces remained stable. Because the normal load is too low to cause the wear or deformation of graphene, the almost unchanged friction force *versus* sliding time on supported graphene and suspended graphene surfaces could be well understood.

We speculated that such a situation for the hillock-like structure was related to the result of the relative sliding at the interface of the SiO_2 substrate and graphene due to the
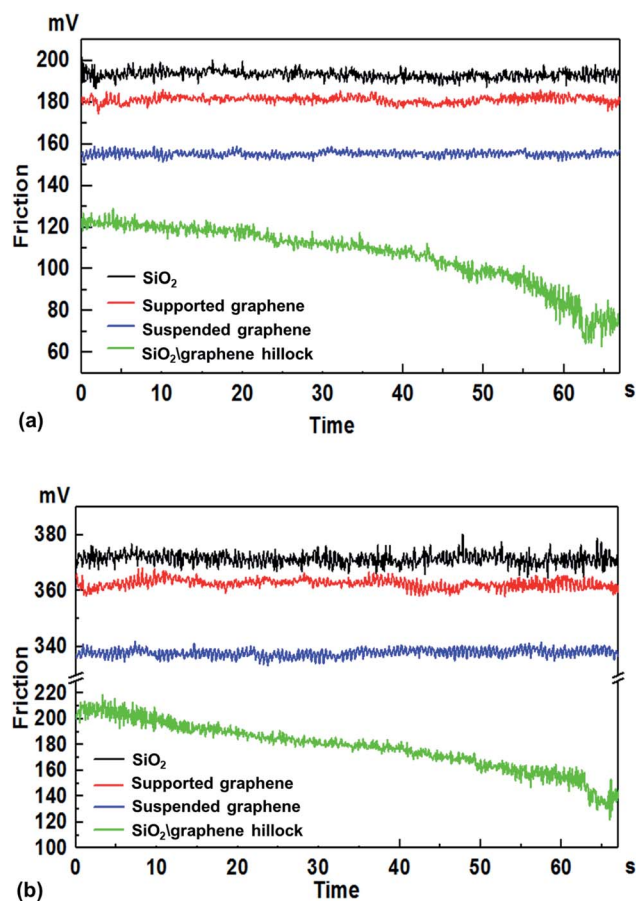

Fig. 7 Measurement of friction force on the SiO_2 substrate, supported graphene, suspended graphene and the hillock-like structure on the SiO_2/graphene surface under the normal loads of 5 nN (a) and 10 nN (b).

movement of the AFM tip. Fig. 8 shows the model of the friction structure when relative sliding occurred at the interface of graphene and the substrate; from top to bottom: AFM tip (A), graphene (B), and SiO_2 substrate (C). When the AFM tip moves in a certain direction with a velocity v, the force analysis of A, B, and C in the lateral direction is as presented in this figure. To analyse the resultant force of graphene, the following relationships should be satisfied:

$$F_B = F_{AB} + F_{CB} = m_B \alpha_B \qquad (1)$$

where F_{AB} represents the tangential force of the AFM tip on graphene and F_{CB} represents the tangential force of the SiO_2 substrate on graphene. Eqn (1) shows that the resultant tangential force on graphene is equal to the sum of the tangential force from the tip and the tangential force from the substrate. Because graphene was of rather low quality and the AFM tip maintained a uniform motion, the acceleration of the graphene would gradually approach zero, suggesting that the tangential force of the tip on the graphene is equal to the tangential force of the SiO_2 substrate on graphene, namely:

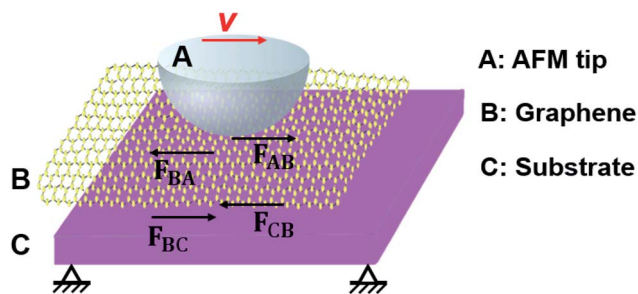$$F_{AB} = F_{CB} \qquad (2)$$

Fig. 8 Schematic diagram showing the friction behavior of the AFM tip/graphene/SiO$_2$ substrate when a relative sliding occurs at the interface of graphene and the SiO$_2$ substrate.

Fig. 9 (a) Adhesion force map covering the SiO$_2$ substrate, the supported graphene, the suspended graphene, and the hillock-like structure on the SiO$_2$/graphene surface. (b) Statistics of the adhesion force on the above four surfaces.

Thus, it is suggested that the tangential force on the hillock-like structure surface (the curve with the green colour in Fig. 7) equalled the tangential force of graphene on the SiO$_2$ substrate. The initial friction force value of the hillock-like structure surface is the lowest compared to other cases as shown in Fig. 7, which is in agreement with the experimental results reported by Liu *et al.*[12] This study reveals that the friction force of the graphene-coated SiO$_2$ tip (that is, graphene grown directly on the SiO$_2$ microsphere surface) against the SiO$_2$ substrate is much lower than that of the SiO$_2$ tip against the graphene substrate. Our experiment showed that the friction force of the hillock-like structure surface was lower than that of the suspended graphene, which could prove the existence of the relative sliding occurring at the interface of the graphene and SiO$_2$ substrate. During the continuous rubbing process with the AFM tip, the adhesion strength between graphene and the substrate was gradually weakened along with the relative motion of graphene and the substrate, resulting in the continued decrease in the friction resistance of graphene. This phenomenon was reflected in the experiment, that is, the measured friction force value gradually decreased *versus* sliding time (show in Fig. 7).

(III) Formation of the hillock-like structure by deformed SiO$_2$

In order to illustrate what the SiO$_2$/graphene hillock-like structure is, deformed SiO$_2$ or a combination of puckering graphene and the deformed SiO$_2$, we conduct the adhesion force test. Fig. 9a and b show the difference of adhesion force on the four different surfaces, which indicates that (i) the adhesion force on the SiO$_2$ surface ($\sim$108 nN) was much higher than those on the other three surfaces; (ii) the adhesion force on the supported graphene surface and the suspended graphene (without the substrate effect) was similar ($\sim$50 nN), indicating that the SiO$_2$ substrate had a little influence on the adhesion force in our experiment; and (iii) it is notable that the hillock-like structure surface showed the lowest adhesion force ($\sim$10 nN).

It is well known that the adhesion force is mainly the van der Waals force, consisting of the Keesom, Debye, and London dispersion forces[34] where the London dispersion force (as a result of two instantaneously induced dipoles acting on each other) plays a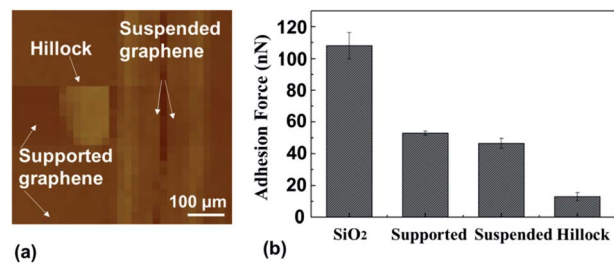 dominant role. The previous results have already shown that when graphene and its SiO$_2$ substrate adhered well with no relative sliding occurring on their interface, the distribution of graphene dipoles did not change, compared to the suspended graphene without the substrate. Hence, the supported graphene surface and the suspended graphene exhibited a similar value of adhesion force, as already shown in Fig. 9. Nevertheless, the significant decrease in the adhesion force of the hillock-like structure surface was related to the change in the distribution of graphene dipoles induced by the friction at these interfaces. In fact, SiO$_2$ is a polarisable material and the electrostatic interaction between graphene and the SiO$_2$ substrate has been described.[35] By analysing the electrostatic interactions between monolayer graphene and a SiO$_2$ substrate, Sabio *et al.*[36] found that the polar modes on the SiO$_2$ surface and the water molecules between graphene and SiO$_2$ were the main factors affecting the electrostatic interaction between graphene and substrate. Given that our experiments were conducted in an air environment, after relative sliding at the graphene/SiO$_2$ interface induced by the AFM tip, either polar modes of SiO$_2$ or water molecules in the air directly affected the distribution of graphene dipoles during the friction process, as shown in Fig. 10. Therefore, the much lower adhesion of the hillock-like structure not only suggested that a relative movement had occurred between graphene and the SiO$_2$ substrate in our experiment, but also proved that the SiO$_2$/graphene hillock-like structure was generated by the deformation of the SiO$_2$ substrate since the electrostatic interaction can only occur between graphene and SiO$_2$. If there is puckering graphene, the adhesion force of the hillock-like structure should be the same as that of the suspended graphene.
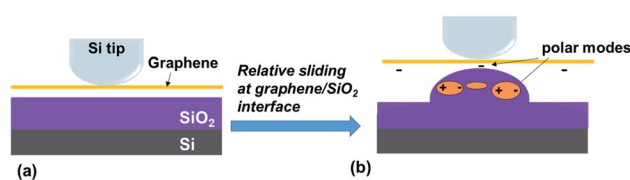

Fig. 10 Interaction with polar modes at the interface of graphene and the SiO$_2$ substrate before (a) and after (b) the relative sliding occurring at the interface.

Conclusions

With its ultra-high strength and bearing capacity, graphene can form a continuous transfer film with self-lubrication and high bonding properties by combining with other materials, which is beneficial for reducing the friction coefficient and improving wear resistance. However, graphene does not always adhere well to many substrates, and the adhesion strength of graphene to its substrate can be easily weakened during the friction process, even resulting in ultimate failure. Nevertheless, the vast majority of experiments on graphene coating are carried out in the case of the strong adhesion of graphene to the substrate, rather than with a weak adhesion of graphene to the substrate.

In this study, the main purpose was to examine the tribological properties of the graphene surface when the adhesion of graphene to the SiO_2 substrate was weakened, as well as the interaction between graphene and its substrate. First, we designed an experiment to weaken the adhesion between graphene and the SiO_2 substrate. Second, the graphene with a weakened adhesion to its substrate was rubbed with an AFM tip and it was found that the monolayer graphene as a coating lost its protective effect on the SiO_2 substrate, such that the structure was deformed, even damaged, in the SiO_2 substrate. The AFM tip and the covered graphene with weak adhesion to SiO_2 substrate together rubbed the SiO_2 substrate, prompting the formation of a higher hillock-like structure with a height of approximately tens of nanometers on the SiO_2/graphene surface. Moreover, we found that tribological properties such as friction and adhesion forces of SiO_2/graphene hillock-like structures were significantly different from those of the original SiO_2/graphene surface, that is, the hillock-like structure exhibited very a low adhesion and a continuously decreasing friction force *versus* sliding time. Compared with the hillock-like structure on the bare SiO_2 surface as well as combined with the proposed force model, we demonstrated that with the emergence of the hillock-like structure, very low adhesion and continuously decreasing friction was induced by the relative sliding at the graphene/substrate interface by the movement of the AFM tip.

To sum up, this work revealed the possibility of the occurrence of relative sliding at the interface of graphene and the SiO_2 substrate when graphene weakly adheres to its substrate, along with a formation of a hillock-like structure on the SiO_2/graphene surface. This finding suggests a potential failure of the graphene coating when the adhesion strength between graphene and its substrate is weakened. Conversely, it provides a possibility for *in situ* fabrication of the low friction and adhesion hillock structure on the SiO_2/graphene surface that could be applied in micro- and nano-devices.

Experimental section

Growth of monolayer graphene using the CVD technique

The monolayer graphene film was grown using the chemical vapour deposition (CVD) method on a 25 μm thick 99.8% copper foil.[37] We placed the copper foil in a CVD furnace and heated it to 985 °C for 20 min with CH_4 (35 sccm) and H_2 (2 sccm) as the sources, in a vacuum of 500 mTorr. After the growth, the sample was cooled until the temperature decreased to less than 100 °C. We confirmed by Raman spectroscopy that the monolayer graphene film was grown on the Cu foil.

Wet transfer of graphene. We carried out a standard graphene transfer technique using polymethyl methacrylate (PMMA) films as the transfer substrates.[38] In the transfer process, first, a thin layer of PMMA was spin-coated on the graphene/Cu substrate. The Cu foil was then etched away by dipping in an $FeCl_3$ solution for more than 12 h. The PMMA/graphene sheets were rinsed with deionised water three times and finally transferred onto the patterned SiO_2/Si substrates, which were fabricated using the focused ion beam (FIB) technique. PMMA was later dissolved using acetone.

AFM experiments. We used AFM to characterise the surface topography of the samples, measure the adhesion and friction forces, and perform the indentation and scratching tests. Thus, AFM images, adhesion force, and parts of frictional forces were obtained using Si_3N_4 tips with radii of $\sim$20 nm and spring constant k_1 of the cantilever of $\sim$0.08 N m^{-1}. To perform indentation and scratching tests, we used Si tips with a higher spring constant k_2 of $\sim$40 N m^{-1}. The experiments were carried out in an atmospheric environment with a temperature of $\sim$25 °C and relative humidity of $\sim$45%. The surface topography of the samples was scanned by these AFM probes in contact mode, and then adhesion and frictional forces were measured *in situ* by AFM.

AFM image processing. All of the AFM images are processed using the Pico View (2D) and Pico Image Basic (3D) software of the AFM system. The step of "flatten" should be done for every image first to ensure the image of the sample is horizontal. The ups and downs of the sample are expressed by the relative color of the image. Generally, a lighter color means a higher height. The size of the image can be cut on purpose, and a scale should be present on the final image.

Conflicts of interest

The authors declare no conflict of interest.

Acknowledgements

References

1 J. S. Choi, J. S. Kim, I. S. Byun, D. H. Lee, M. J. Lee, B. H. Park, C. Lee, D. Yoon, H. Cheong, K. H. Lee, Y. W. Son, J. Y. Park and M. Salmeron, *Science*, 2011, **333**, 607–610.

2 H. Xiao and S. Liu, *Mater. Des.*, 2017, **135**, 319–332.

3 L. Liu, M. Zhou, X. Li, L. Jin, G. Su, Y. Mo, L. Li, H. Zhu and Y. Tian, *Materials*, 2018, **11**, 1314.

4 C. Lee, Q. Li, W. Kalb, X. Z. Liu, H. Berger, R. W. Carpick and J. Hone, *Science*, 2010, **328**, 79–80.

5 K. S. Kim, H. J. Lee, C. Lee, S. K. Lee, H. Jang, J. H. Ahn, J. H. Kim and H. J. Lee, *ACS Nano*, 2011, **5**, 5107–5144.

6 D. Berman, A. Erdemir and A. V. Sumant, *Mater. Today*, 2014, **17**, 31–42.

7 Y. T. Peng, Z. Q. Wang and K. Zou, *Langmuir*, 2015, **31**, 7782–7791.

8 X. Y. Ge, J. J. Li, H. D. Wang, C. H. Zhang, Y. H. Liu and J. B. Luo, *Carbon*, 2019, **151**, 76–83.

9 Z. Deng, N. N. Klimov, S. D. Solares, T. Li, H. Xu and R. J. Cannara, *Langmuir*, 2013, **29**, 235–243.

10 H. Deng, M. Ma, Y. M. Song, Q. C. He and Q. S. Zheng, *Nanoscale*, 2017, 1–6.

11 D. Berman, S. A. Deshmukh, S. K. R. S. Sankaranarayanan, A. Erdemir and A. V. Sumant, *Science*, 2015, **348**, 1118–1122.

12 S. W. Liu, H. P. Wang, Q. Xu, T. B. Ma, G. Yu, C. H. Zhang, D. C. Geng, Z. W. Yu, S. G. Zhang, W. Z. Wang, Y. Z. Hu, H. Wang and J. B. Luo, *Nat. Commun.*, 2017, **8**, 14029.

13 X. H. Zheng, L. Gao, Q. Z. Yao, Q. Y. Li, M. Zhang, X. M. Xie, S. Qiao, G. Wang, T. B. Ma, Z. F. Di, J. B. Luo and X. Wang, *Nat. Commun.*, 2016, **7**, 13204.

14 Y. M. Liu, A. S. Song, Z. Xu, R. L. Zong, J. Zhang, W. Y. Yang, R. Wang, Y. Z. Hu, J. B. Luo and T. B. Ma, *ACS Nano*, 2018, **12**, 7638–7646.

15 X. Z. Zeng, Y. T. Peng and H. J. Lang, *Carbon*, 2017, **118**, 233–240.

16 X. Z. Zeng, Y. T. Peng, H. J. Lang and L. Liu, *Sci. Rep.*, 2017, **7**, 41891.

17 J. Torres, Y. Zhu, P. Liu, S. C. Lim and M. Yun, *Phys. Status Solidi*, 2018, **215**, 1700512.

18 Y. T. Peng, X. Z. Zeng, L. Liu, X. G. Cao, K. Zou and R. Chen, *Carbon*, 2017, **124**, 541–546.

19 Z. Zong, C. L. Chen, M. R. Dokmeci and K. T. Wan, *J. Appl. Phys.*, 2010, **107**, 026104.

20 G. Paolicelli, M. Tripathi, V. Corradini, A. Candini and S. Valeri, *Nanotechnology*, 2015, **26**, 055703.

21 J. S. Bunch and M. L. Dunn, *Solid State Commun.*, 2012, **152**, 1359–1364.

22 A. C. Ferrari, F. Bonaccorso, V. Fal'ko, K. S. Novoselov, S. Roche, P. Bøggild, S. Borini, F. H. L. Koppens, V. Palermo, N. Pugno, J. A. Garrido, R. Sordan, A. Bianco, L. Ballerini, M. Prato, E. Lidorikis, J. Kivioja, C. Marinelli, T. Ryhänen, A. Morpurgo, J. N. Coleman, V. Nicolosi, L. Colombo, A. Fert, M. Garcia-Hernandez, A. Bachtold, G. F. Schneider, F. Guinea, C. Dekker, M. Barbone, Z. Sun, C. Galiotis, A. N. Grigorenko, G. Konstantatos, A. Kis, M. Katsnelson, L. Vandersypen, A. Loiseau, V. Morandi, D. Neumaier, E. Treossi, V. Pellegrini, M. Polini, A. Tredicucci, G. M. Williams, B. Hee Hong, J.-H. Ahn, J. Min Kim, H. Zirath, B. J. van Wees, H. van der Zant, L. Occhipinti, A. Di Matteo, I. A. Kinloch, T. Seyller, E. Quesnel, X. Feng, K. Teo, N. Rupesinghe, P. Hakonen, S. R. T. Neil, Q. Tannock, T. Löfwander and J. Kinaret, *Nanoscale*, 2015, **7**, 4598–4810.

23 S. Das, D. Lahiri, D. Y. Lee, A. Agarwal and W. Choi, *Carbon*, 2013, **59**, 121–129.

24 C. F. Song, X. Y. Li, B. J. Yu, H. S. Dong, L. M. Qian and Z. R. Zhou, *Nanoscale Res. Lett.*, 2011, **6**, 310.

25 B. J. Yu, H. S. Dong, L. M. Qian, Y. F. Chen, J. X. Yu and Z. R. Zhou, *Nanotechnology*, 2009, **20**, 465303.

26 P. Gong, Z. J. Ye, L. Yuan and P. Egberts, *Carbon*, 2018, **132**, 749–759.

27 H. Lee, J. H. Ko, J. S. Choi, J. H. Hwang, Y. H. Kim, M. Salmeron and J. Y. Park, *J. Phys. Chem. Lett.*, 2017, **8**, 3482–3487.

28 Y. Z. Qi, J. Liu, J. Zhang, Y. L. Dong and Q. Y. Li, *ACS Appl. Mater. Interfaces*, 2016, **9**, 1099–1106.

29 N. Fan, Z. Z. Ren, G. Y. Jing, J. Guo, B. Peng and H. Jiang, *Materials*, 2017, **10**, 164.

30 F. Zheng and F. L. Duan, *Tribol. Int.*, 2019, **134**, 87–92.

31 A. P. M. Barboza, H. Chacham, C. K. Oliveira, T. F. D. Fernandes, E. H. Martins Ferreira, B. S. Archanjo, R. J. C. Batista, A. B. de Oliveira and B. R. A. Neves, *Nano Lett.*, 2012, **12**(5), 2313–2317.

32 C. Lee, Q. Li, W. Kalb, X. Z. Liu, H. Berger, R. W. Carpick and J. Hone, *Science*, 2010, **328**(5974), 76–80.

33 Q. Li, C. Lee, R. W. Carpick and J. Hone, *Phys. Status Solidi B*, 2010, **247**(11–12), 2909–2914.

34 Z. X. Lu and M. L. Dunn, *J. Appl. Phys.*, 2010, **107**, 044301.

35 W. H. Wang, R. X. Du, A. Zafar, L. P. He, W. W. Zhao, Y. F. Chen, J. P. Lu and Z. H. Ni, *IEEE Electron Device Lett.*, 2017, **38**, 1136–1138.

36 J. Sabio, C. Seoánez, S. Fratini, F. Guinea, A. H. Castro Neto and F. Sols, *Phys. Rev. B: Condens. Matter Mater. Phys.*, 2008, **77**, 195409.

37 Y. Bie, Y. Zhou, Z. Liao, K. Yan, S. Liu, Q. Zhao, S. Kumar, H. Wu, G. S. Duesberg, G. L. W. Cross, J. Xu, H. Peng, Z. Liu and D. Yu, *Adv. Mater.*, 2011, **23**, 3938–3943.

38 J. J. Chen, J. Meng, D. Yu and Z. Liao, *Sci. Rep.*, 2014, **4**, 5065.